Tian et al. Nanoscale Research Letters (2016) 11:219
DOI 10.1186/s11671-016-1433-6

Nanoscale Research Letters

NANO EXPRESS Open Access

Creation and Transfer of Coherence via Technique of Stimulated Raman Adiabatic Passage in Triple Quantum Dots

Si-Cong Tian[1*], Ren-Gang Wan[2], Chun-Liang Wang[3], Shi-Li Shu[1], Li-Jie Wang[1] and Chun-Zhu Tong[1*]

Abstract

We propose a scheme for creation and transfer of coherence among ground state and indirect exciton states of triple quantum dots via the technique of stimulated Raman adiabatic passage. Compared with the traditional stimulated Raman adiabatic passage, the Stokes laser pulse is replaced by the tunneling pulse, which can be controlled by the externally applied voltages. By varying the amplitudes and sequences of the pump and tunneling pulses, a complete coherence transfer or an equal coherence distribution among multiple states can be obtained. The investigations can provide further insight for the experimental development of controllable coherence transfer in semiconductor structure and may have potential applications in quantum information processing.

Keywords: Triple quantum dots, Creation and transfer of coherence, Stimulated Raman adiabatic passage

Background

Atomic coherence has attracted considerable interest in recent years because atomic coherence is essential for many effects, such as electromagnetically induced transparency (EIT) [1–3], laser without inversion [4–6], coherent population transfer [7–10], and subluminal and superluminal light propagation [11, 12]. The technique of stimulated Raman adiabatic passage (STIRAP) can be used for coherent controlling of an atomic system to a particular state, both in a Λ-type three-level system [13, 14] and in a multiple-level system [15–19]. And by fractional STIRAP (F-STIRAP), creation of atomic coherence can be obtained [20]. Besides, in a Λ-type system where the final state has twofold states, creation of atomic coherence by STIRAP is also possible because of the double dark states induced by the control laser [21].

On the other hand, quantum dots (QDs) have three-dimensional confinement of carriers, which makes the holes and electrons in QDs only occupy the discrete-energy states. Compared with atoms, QDs have larger electric-dipole moments and higher nonlinear optical coefficients. Besides, the other advantages of QDs over atoms are their flexible designed energy scales and physical features, proper selection of the materials and the sizes, and customized design and ease of integration. Thus, QDs are widely used to perform atomic coherence experimental and theoretical investigations in solid-state structures. For instance, coherent manipulation population [22–25] and other coherent phenomena [26–28] in QDs have been reported.

The next natural step is to couple two closely spaced QDs together. By the self-assembled dot growth method, double quantum dots (DQDs) can be fabricated [29]. In DQDs, the tunneling between the inter dots can be controlled not only by the composition but also by the externally applied voltages; thus, DQDs are an ideal system for experimental and theoretical investigations, where the interactions between light and matter can be fully controlled and coherence characteristics can be probed by electrical and optical methods. Therefore, many studies concentrate on generating and employing the coherence in DQDs [30–40]. Based on DQDs, triple quantum dots (TQDs) have been fabricated in many processes [41–44]. The electron and hole confinement, as well as the intermediate band of such quantum dot molecules, have been studied [45, 46]. And TQDs can bring in multilevel structure and

* Correspondence: tiansicong@ciomp.ac.cn; tongcz@ciomp.ac.cn
[1]State Key Laboratory of Luminescence and Applications, Changchun Institute of Optics, Fine Mechanics and Physics, Chinese Academy of Sciences, Changchun 130033, China
Full list of author information is available at the end of the article

extra controlling parameters which cannot be found in DQDs [47–49].

We note that the coherent population transfer can be realized in a three-level QD system with more than one dot [50–52]. But to our knowledge, there is no investigation on transferring and manipulating of coherence. So in this paper, we propose a scheme for controlling coherence transfer among ground state and indirect exciton states of TQDs via the technique of STIRAP. Compared with the traditional STIRAP, the Stokes laser pulse is replaced by the tunneling pulse, which can be controlled by the externally applied voltages. We show that a complete coherence transfer or an equal coherence distribution among multiple states can be obtained via the pump and tunneling pulses with different amplitudes and sequences. Our investigations can provide further insight for the experimental development of controllable coherence transfer in semiconductor structure and may have potential applications in quantum information processing.

Methods

The TQD system consists of three QDs, which have different band structures and are arranged triangularly, as shown in Fig. 1a. In such system, the tunneling barrier depends on the gate electrode between the three QDs. When the gate voltage is not applied, the conduction-band electron energy levels are out of resonance; therefore, the electron tunneling between the neighbor QDs is quite weak. On the contrary, when the gate voltage is applied, the conduction-band electron energy levels are resonant; therefore, the electron tunneling between the neighbor QDs becomes very strong. The hole tunneling is neglected due to the off-resonance of the valence-band energy levels in the latter situation.

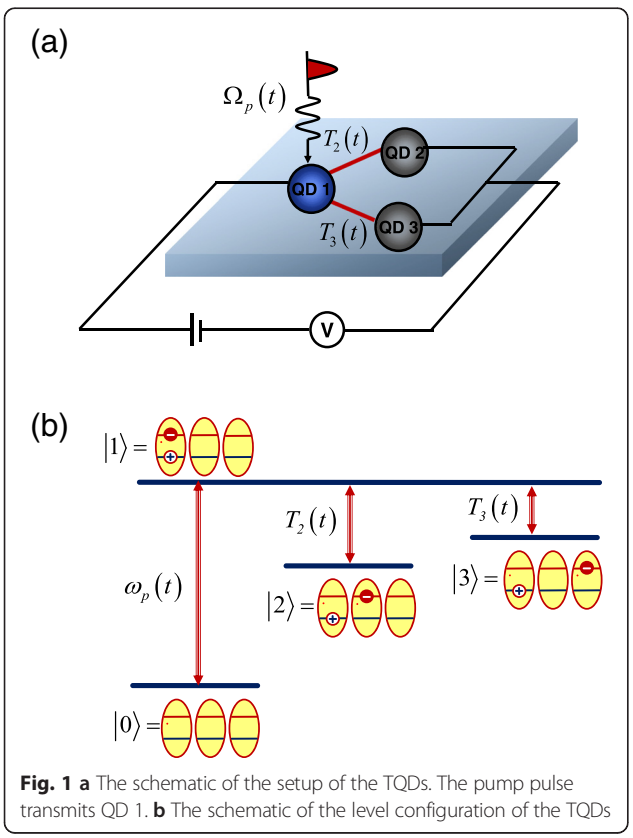

Fig. 1 **a** The schematic of the setup of the TQDs. The pump pulse transmits QD 1. **b** The schematic of the level configuration of the TQDs

Under the resonant coupling of a pump laser field with QD1, an electron is excited in QD1. Then with the tunneling, the electron can be transferred to QD2 and QD3. Thus, the TQD structure can be treated as a four-level tripod system (Fig. 1b): the ground state $|0\rangle$, where there is no excitations in any QD, the direct exciton state $|1\rangle$, where the electron and hole are both in the first QD, the indirect exciton state $|2\rangle$, where the electron is in the second dot and the hole remains in the first dot, and the indirect exciton state $|3\rangle$, where the electron is in the third dot and the hole remains in the first dot.

At any time t, the state vector can be written as

$$|\Psi(t)\rangle = a_0(t)|0\rangle + a_1(t)|1\rangle + a_2(t)|2\rangle + a_3(t)|3\rangle. \quad (1)$$

The time evolution of the probability amplitude $A(t) = [a_0(t), a_1(t), a_2(t), a_3(t)]^T$ of the four states is described by the Schrödinger equation

$$\frac{d}{dt}A(t) = -\frac{i}{\hbar}H(t)A(t) - \Lambda A(t), \quad (2)$$

where $H(t)$ is the Hamiltonian of TQDs and Λ is the dissipative process containing spontaneous decay process and the pure dephasing. In the rotating-wave approximation, the expression of $H(t)$ under the coupling of the pump and tunneling pulses can be written as

$$H(t) = \hbar \begin{pmatrix} 0 & \Omega_p(t) & 0 & 0 \\ \Omega_p(t) & -\delta_p & T_2(t) & T_3(t) \\ 0 & T_2(t) & -(\delta_p - \omega_{12}) & 0 \\ 0 & T_3(t) & 0 & -(\delta_p - \omega_{13}) \end{pmatrix}. \quad (3)$$

Here, $\Omega_p(t)$ is the Rabi frequency of the pump pulse, and $T_2(t)$ and $T_3(t)$ are the tunneling pulses, which can be controlled by varying the bias voltage. In our calculations, Ω_p, T_2, and T_3 denote the peak value of the pump pulse and two tunneling pulses, and all the pulses have the same pulse duration T. The energy splitting of the direct exciton state $|1\rangle$ and ground state $|0\rangle$ is ω_{10}, and the energy splitting of the direct exciton state $|1\rangle$ and indirect exciton states $|2\rangle$ and $|3\rangle$ are ω_{12} and ω_{13}, respectively. $\delta_p = \omega_{10} - \omega_p$ denotes the pump detuning (ω_p is the frequency of the pump pulse). And in TQDs, the energy splitting depends on the effective confinement potential and are much smaller than ω_{10}.

Substituting Eq. (1) and Eq. (3) into Eq. (2), we can obtain the following dynamical equations for atomic probability amplitudes in the interaction picture:

$$i.a_0 = -\Omega_p a_1, \tag{4a}$$

$$i.a_1 = -\Omega_p a_0 - T_2 a_2 - T_3 a_3 + (\delta_p - i\gamma_1) a_1, \tag{4b}$$

$$i.a_2 = -T_2 a_1 + (\delta_p - \omega_{12} - i\gamma_2) a_2, \tag{4c}$$

$$i.a_3 = -T_3 a_1 + (\delta_p - \omega_{13} - i\gamma_3) a_3, \tag{4d}$$

Here, $\gamma_i = \frac{1}{2}\Gamma_{i0} + \gamma_{i0}^d \ (i = 1\text{–}3)$ is the typical effective decay rate, with Γ_{i0} being the radiative decay rate of populations from $|i\rangle \rightarrow |0\rangle$ and γ_{i0}^d being the pure dephasing rates.

The time evolutions of population and the coherence dynamics can be calculated by the density matrix element $|\rho_{ij}| = |a_i^* a_j|$. If $i = j$, $|\rho_{ij}|$ represents the time evolutions of population P_i, while if $i \neq j$, $|\rho_{ij}|$ represents the coherence dynamics.

In our calculations, the realistic values of TQD parameters are $\hbar T_{2,3} \sim 1\text{–}10$ meV, $\hbar\gamma_1 \sim 0.002\text{–}0.01$ meV, and $\gamma_2 = \gamma_3 = 10^{-3}\gamma_1$ [47]. And for simplicity, δ_p, ω_{12}, and ω_{13} are set to 0. With these parameters, the adiabatic condition can be fully satisfied. And in all the cases, the initial population is assumed to be in state $|0\rangle$, that is $a_0(-\infty) = 1$, $a_{1,2,3}(-\infty) = 0$.

Results and Discussion

Our first task is to achieve coherence transfer in TQDs, and we show the corresponding results in Fig. 2. In step I, we prepare the coherence between states $|0\rangle$ and $|2\rangle$ by a F-STIRAP among states $|0\rangle$, $|1\rangle$, and $|2\rangle$. With the tunneling pulse $T_2(t)$ and the pump pulse $\Omega_p(t)$, the system state vector in step I goes to

$$|\Psi_I\rangle = \cos\theta|0\rangle - \sin\theta|2\rangle, \tag{5a}$$

$$\tan\theta = \frac{\Omega_p(t)}{T_2(t)}. \tag{5b}$$

Here, the mixing angle θ is similar to the conventional one defined in STIRAP of a Λ atomic system. From Eq. (5a), state $|\Psi_I\rangle$ has no component of state $|1\rangle$, which indicates that it does not arouse the stimulated emission from state $|1\rangle$ to $|0\rangle$ in step I. Furthermore, from Eq. (5a), the coherence amplitude between states $|0\rangle$ and $|2\rangle$ can be calculated, which is

$$|\rho_{02}| = |\cos\theta \sin\theta|. \tag{6}$$

Hence, by tuning the mixing angle θ, arbitrary intensity of coherence between states $|0\rangle$ and $|2\rangle$ can be obtained. If $T_2(t)$ precedes $\Omega_p(t)$, and they have the same amplitude and are switched off simultaneously, as time progresses from 0 to ∞, the value of $\Omega_p(t)/T_2(t)$ rises from 0 to 1, and consequently, the mixing angle θ rises from 0 to $\pi/4$. As a result, the adiabatic state $|\Psi_I\rangle$ starting in the bare state $|0\rangle$ will end in the coherent superposition state $|\Psi_I\rangle = (|0\rangle - |2\rangle)/\sqrt{2}$. This means that the maximal coherence between states $|0\rangle$ and $|2\rangle$ is obtained.

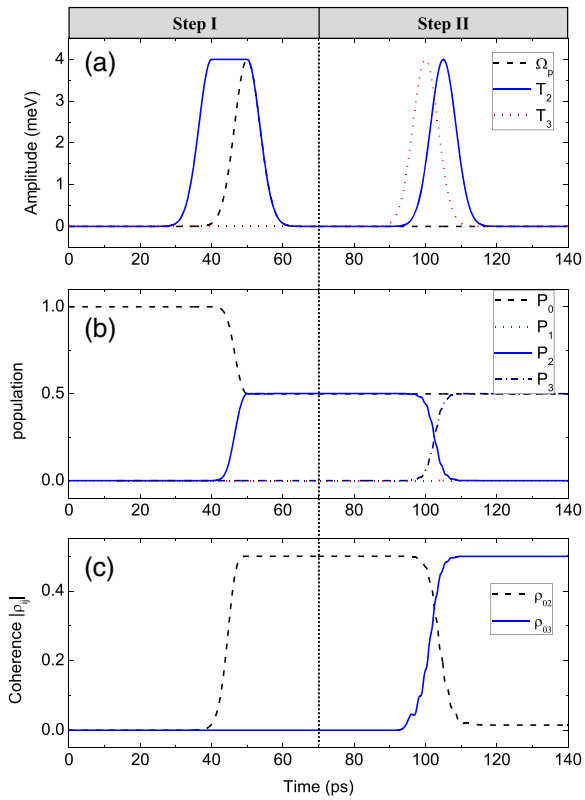

Fig. 2 **a** The pump and the tunneling pulses. **b** The time evolutions of population $P_i = |a_i|^2$ ($i = 0\text{–}3$). **c** The coherence dynamics $|\rho_{ij}|$. In step I, the peak values of $\hbar\Omega_p$ and $\hbar T_2$ are both 4 meV. In step II, the peak values of $\hbar T_2$ and $\hbar T_3$ are both 4 meV. Other parameters are $\delta_p = \omega_{12} = \omega_{13} = 0$, $\hbar\gamma_1 = 0.01$ meV, and $\gamma_2 = \gamma_3 = \gamma_4 = 10^{-3}\gamma_1$

We give numerical simulation to illustrate the time evolutions of the system in step I. The tunneling pulse $T_2(t)$ and the pump pulse $\Omega_p(t)$ are plotted in the left column of Fig. 2a. Then, the time evolutions of the population $P_i = |a_i|^2$ ($i = 0\text{–}3$) and the coherence dynamics $|\rho_{02,03}|$ can be drawn in the left column of Fig. 2b, c, respectively. As the left column of Fig. 2b reveals, the population is distributed equally in two states $|0\rangle$ and $|2\rangle$ at the end of step I. And state $|1\rangle$ is empty in the whole process. It can be seen from the left column of Fig. 2c that $|\rho_{02}|$ arises from 0 to the maximum value 1/2 during step I. Because $T_3(t)$ is switched off, the population P_3 and the coherence $|\rho_{03}|$ remain 0.

Now, we have the coherence between states $|0\rangle$ and $|2\rangle$. Then in step II, we will transfer this coherence to that between states $|0\rangle$ and $|3\rangle$ by a STIRAP process among states $|1\rangle$, $|2\rangle$, and $|3\rangle$. In this process, $\Omega_p(t)$ is

switched off and both tunneling pulses $T_2(t)$ and $T_3(t)$ are switched on. Because the probability amplitude of $|0\rangle$ is unchanged, and the probability amplitude of $|2\rangle$ is changed to the superposition states of $|2\rangle$ and $|3\rangle$, the system state vector goes to

$$|\Psi_{II}\rangle = \cos\theta|0\rangle - \sin\theta(\cos\phi|2\rangle - \sin\phi|3\rangle), \tag{7a}$$

$$\tan\phi = \frac{T_2(t)}{T_3(t)}. \tag{7b}$$

Here, ϕ is the other mixing angle relative to two tunneling pulses in the STIRAP process. From Eq. (7a), the state $|\Psi_{II}\rangle$ has no component of the state $|1\rangle$ either, so it does not arouse the stimulated emission from state $|1\rangle$ to state $|0\rangle$ in step II. Also from Eq. (7a), the amplitudes of the possible coherence can be calculated

$$|\rho_{02}| = |\cos\theta \sin\theta \cos\phi|, \tag{8a}$$

$$|\rho_{03}| = |\cos\theta \sin\theta \sin\phi|, \tag{8b}$$

$$|\rho_{23}| = |\sin^2\theta \cos\phi \sin\phi|. \tag{8c}$$

Hence, by tuning the mixing angle, the coherence among states $|0\rangle$, $|2\rangle$, and $|3\rangle$ with arbitrary value can be obtained. If $T_3(t)$ precedes $T_2(t)$ with the same amplitude, and they overlap in the process, as time progresses from 0 to ∞, the value of $T_2(t)/T_3(t)$ rises from 0 to ∞, and consequently, the mixing angle ϕ rises from 0 to $\pi/2$. Together with $\theta = \pi/4$ (step I), the final adiabatic state $|\Psi_{II}\rangle$ will end in the coherent superposition state $|\Psi_{II}\rangle = (|0\rangle + |3\rangle)/\sqrt{2}$. This means that the maximal coherence between states $|0\rangle$ and $|3\rangle$ is obtained.

We give numerical simulation to illustrate the time evolutions of the system in step II. The tunneling pulses $T_2(t)$ and $T_3(t)$ are plotted in the right column of Fig. 2a. Then, the time evolutions of the population $P_i = |a_i|^2$ $(i = 0–3)$ and the coherence dynamics $|\rho_{02,03}|$ are shown in the right column of Fig. 2b, c, respectively. As can be seen in the right column of Fig. 2b, the population in state $|2\rangle$ is completely transferred to state $|3\rangle$, while the population in state $|0\rangle$ is unchanged. In the whole process, state $|1\rangle$ keeps empty. Furthermore, the right column of Fig. 2c reveals that the coherence between states $|0\rangle$ and $|2\rangle$ is fully transferred to that between states $|0\rangle$ and $|3\rangle$, with the maximum value being 1/2 at the end of step II.

Now, we focus our attention on how to control the coherence distribution in TQDs. We show the corresponding results in Fig. 3. Step I is to prepare the coherence between states $|0\rangle$ and $|2\rangle$. Here, we use the F-STIRAP among states $|0\rangle$, $|1\rangle$, and $|2\rangle$ and the pulse sequences are shown in the left column of Fig. 3a. Compared with Fig. 2a, the only difference is that the peak value of $\Omega_p(t)$ and $T_2(t)$ is $\Omega_p/T_2 = 3/2$ in Fig. 3a. As time progresses, the population transfers from state $|0\rangle$ to state $|2\rangle$, and P_0 and P_2 finally reach a

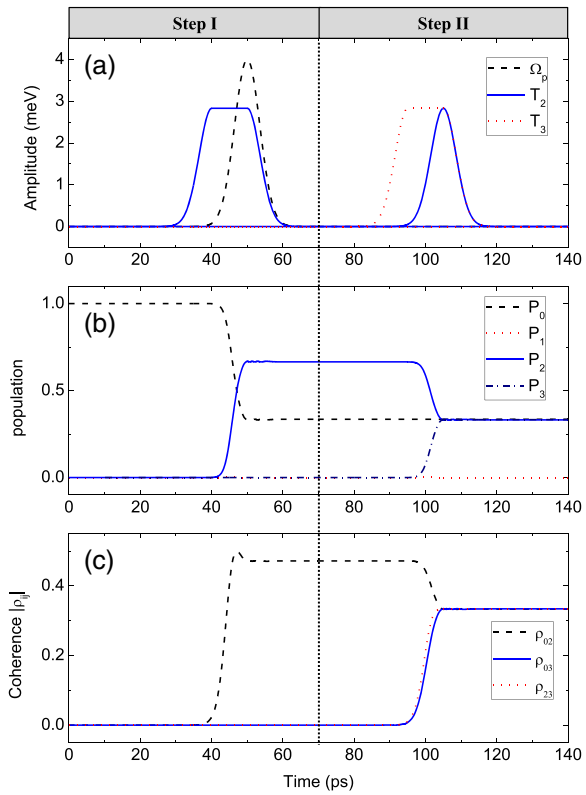

Fig. 3 **a** The pump and the tunneling pulses. **b** The time evolutions of population $P_i = |a_i|^2$ $(i = 0–3)$. **c** The coherence dynamics $|\rho_{ij}|$. In step I, the peak values of $\hbar\Omega_p$ and $\hbar T_2$ are 4 and 2.83 meV, respectively. In step II, the peak values of $\hbar T_2$ and $\hbar T_3$ are both 2.83 meV. Other parameters are the same as those in Fig. 2

stable value with the ratio of $P_2/P_0 = 2$ (left column of Fig. 3b). And the coherence between states $|0\rangle$ and $|2\rangle$ is also obtained, with the value of $|\rho_{02}|$ being a little smaller than the maximum value 1/2 (left column of Fig. 3c).

Step II is to distribute the obtained coherence to that between the desired states. In this process, we use another F-STIRAP process among states $|1\rangle$, $|2\rangle$, and $|3\rangle$ and show the pulse sequences in the right column of Fig. 3a. Both tunneling pulses have the same peak value and time back edge, and the peak value is 2/3 times that of the pump pulse in step I. As time goes, half of the population in state $|2\rangle$ is transferred to state $|3\rangle$, while the population in state $|0\rangle$ is unchanged. At last, the population is equally distributed in these three states $|0\rangle$, $|2\rangle$, and $|3\rangle$. And in the whole step II, state $|1\rangle$ is empty (right column of Fig. 3b). Besides, as can be seen in the right column of Fig. 3c, the value of $|\rho_{02}|$ decreases, while the value of $|\rho_{03}|$ and $|\rho_{23}|$ increases, and at last, all $|\rho_{02}|$, $|\rho_{03}|$, and $|\rho_{23}|$ reach a same stable value 1/3. This means that the coherence obtained in step I is successfully transferred to that between other states.

From Fig. 3, it can be concluded that using the technique of STIRAP, the maximum coherence among three

states $|0\rangle$, $|2\rangle$, and $|3\rangle$ can be realized, with the value of coherence between arbitrary two states being 1/3. While in the usual multiple-level atomic system coupled by continuous-wave laser, the maximum value of coherence between two ground states is only 1/6 [53]. Besides, from Eqs. (6) and (8), the value of $(|\rho_{02}|^2 + |\rho_{03}|^2)^{1/2}$ in step II is equal to that of $|\rho_{02}|$ in step I. In step I, the maximum value of $|\rho_{02}|$ is 1/2; therefore, arbitrary coherence distribution between states $|0\rangle$ and $|2\rangle$ and states $|0\rangle$ and $|3\rangle$ is only limited by $(|\rho_{02}|^2 + |\rho_{03}|^2)^{1/2} \le 1/2$.

The coherence transfer and coherence distribution can also been realized by other pulse sequences and amplitudes, and we show these results in Figs. 4 and 5, respectively. First, we show a complete coherence transfer. In the left column of Fig. 4a, step I prepares the coherence between states $|0\rangle$ and $|2\rangle$ by a F-STIRAP among states $|0\rangle$, $|1\rangle$, and $|2\rangle$, which is the same as step I of Fig. 2. Thus, half of the population is transferred from state $|0\rangle$ to state $|2\rangle$ (left column of Fig. 4b), and the maximum value of coherence between states $|0\rangle$ and $|2\rangle$ is obtained (left column of Fig. 4c). Then in step II, we will transfer the coherence to that between states $|2\rangle$ and $|3\rangle$. Different form Fig. 2, we use a STIRAP among

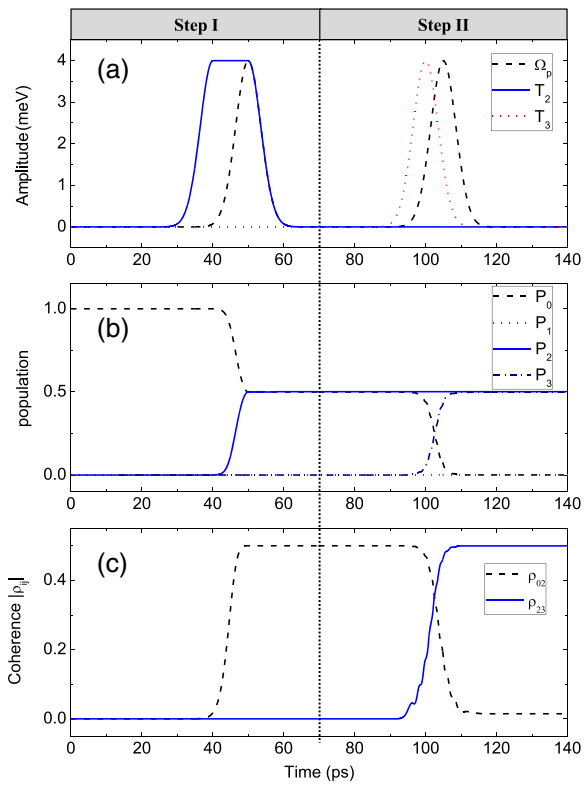

Fig. 4 a The pump and the tunneling pulses. **b** The time evolutions of population $P_i = |a_i|^2$ ($i = 0$–3). **c** The coherence dynamics $|\rho_{ij}|$. In step I, the peak values of $\hbar\Omega_p$ and $\hbar T_2$ are both 4 meV. In step II, the peak values of $\hbar\Omega_p$ and $\hbar T_3$ are both 4 meV. Other parameters are the same as those in Fig. 2

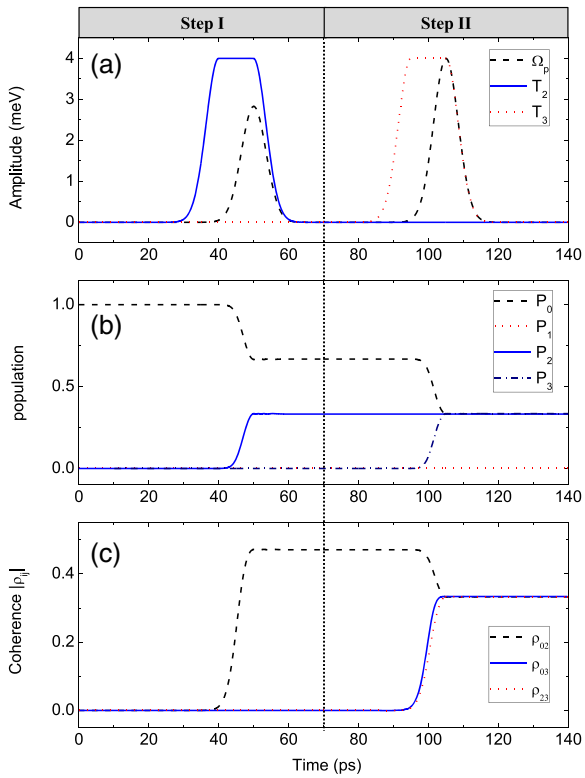

Fig. 5 a The pump and the tunneling pulses. **b** The time evolutions of population $P_i = |a_i|^2$ ($i = 0$–3). **c** The coherence dynamics $|\rho_{ij}|$. In step I, the peak values of $\hbar\Omega_p$ and $\hbar T_2$ are 2.83 and 4 meV, respectively. In step II, the peak values of $\hbar\Omega_p$ and $\hbar T_3$ are both 4 meV. Other parameters are the same as those in Fig. 2

states $|0\rangle$, $|1\rangle$, and $|3\rangle$, rather than states $|1\rangle$, $|2\rangle$, and $|3\rangle$, by applying the pump pulse $\Omega_p(t)$ and tunneling pulse $T_3(t)$. During this process, the probability amplitude of $|2\rangle$ is unchanged, while the probability amplitude of $|0\rangle$ is changed to the superposition states of $|0\rangle$ and $|3\rangle$. In this case, the system state vector goes to

$$|\Psi_{II}\rangle = \cos\theta(\cos\phi|0\rangle - \sin\phi|3\rangle) - \sin\theta|2\rangle, \tag{9a}$$

$$\tan\theta = \frac{\Omega_p(t)}{T_2(t)}, \tag{9b}$$

$$\tan\phi = \frac{\Omega_p(t)}{T_3(t)}. \tag{9c}$$

And as can be seen from Eq. (9a), $|\Psi_{II}\rangle$ has no component of state $|1\rangle$. Here, θ and ϕ are the mixing angles. Then, the amplitudes of the possible coherence are

$$|\rho_{02}| = |\cos\theta \sin\theta \cos\phi|, \tag{10b}$$

$$|\rho_{03}| = |\cos^2\theta \sin\phi \cos\phi|, \tag{10a}$$

$$|\rho_{23}| = |\cos\theta \sin\theta \sin\phi|. \tag{10c}$$

According to Eq. (10), it is possible to control the coherence by tuning the mixing angles. Thus, by using the pulse sequences in the right column of Fig. 4a, the population in state $|0\rangle$ is completely transferred to state $|3\rangle$ (right column of Fig. 4b), and the completed coherence transfer from states $|0\rangle$ and $|2\rangle$ to states $|2\rangle$ and $|3\rangle$ is realized (right column of Fig. 4c).

Next, according to Eq. (10), we present the coherence distribution and show the results in Fig. 5. Step I is to prepare the coherence between states $|0\rangle$ and $|2\rangle$, which can be realized by using the F-STIRAP among states $|0\rangle$, $|1\rangle$, and $|2\rangle$. The pulse sequences with the ratio of the peak value being $\Omega_p/T_2 = 2/3$ are shown in the left column of Fig. 5a. As time progresses, some population transfers from state $|0\rangle$ to state $|2\rangle$ and the final ratio of the population is $P_2/P_0 = 2$ (left column of Fig. 5b). Meanwhile, the maximum coherence between states $|0\rangle$ and $|2\rangle$ is obtained (left column of Fig. 5c). In step II, another F-STIRAP process among states $|0\rangle$, $|1\rangle$, and $|3\rangle$ is used to distribute the obtained coherence. The pulse sequences are shown in the right column of Fig. 5a. As time goes, the population is equally distributed in three states $|0\rangle$, $|2\rangle$, and $|3\rangle$ (right column of Fig. 5b). At the same time, the coherence between states $|0\rangle$ and $|2\rangle$ is equally distributed to that between states $|0\rangle$ and $|2\rangle$, states $|0\rangle$ and $|3\rangle$, and states $|2\rangle$ and $|3\rangle$ (right column of Fig. 5c).

From Figs. 4 and 5, it can be concluded that it is possible to realize coherence transfer and coherence distribution by using other sequences and amplitudes of pump and tunneling pulses. From Eqs. (6) and (10), the value of $(|\rho_{02}|^2 + |\rho_{23}|^2)^{1/2}$ in step II is equal to that of $|\rho_{02}|$ in step I. In step I, the maximum value of $|\rho_{02}|$ is 1/2; therefore, arbitrary coherence distribution between states $|0\rangle$ and $|2\rangle$ and states $|2\rangle$ and $|3\rangle$ is only limited by $(|\rho_{02}|^2 + |\rho_{23}|^2)^{1/2} \le 1/2$. So the limitation of coherence distribution may be different in the condition of the different pulse sequences.

Conclusions

In this paper, we have theoretically demonstrated that it is possible to transfer and manipulate coherence among ground state and indirect exciton states of TQDs by the technique of STIRAP. The whole process can be separated into two steps; in the first step, the creation of coherence between the ground state and one indirect exciton state can be achieved by one process of F-STIRAP. Then in the second step, the complete transfer of coherence between the ground state and the other indirect exciton state can be obtained by the process of STIRAP, or the equal distribution of coherence among the ground state and two indirect exciton states can be obtained by the other process of F-STIRAP. These results can also be obtained by other pump and tunneling pulses with different amplitudes and sequences. Moreover, the value of equal coherence distribution among the multiple states by the technique of STIRAP can reach to 1/3, which is larger than that of using continuous-wave laser. And the only limitation of the coherence distribution is limited by the value of coherence $|\rho_{02}|$ in the first step. Our scheme allows controlling and manipulating coherence in a reliable and flexible way and may have essential applications in quantum information processing based on the atomic coherence effect, such as slow-light storage and quantum logical gates.

Competing Interests

The authors declare that they have no competing interests.

Authors' Contributions

ST and RW conceived the idea and did the calculations. All authors contributed to the discussions about the project and writing of the manuscript. All authors read and approved the final manuscript.

Authors' Information

ST, RW, and CW are associate professors. LW and SS are research assistants. CT is a professor.

Acknowledgements

This work is supported by the financial support from the National Natural Science Foundation of China (Grant Nos. 11304308, 11204029, 11447232, 61176046, and 61234004), the National Basic Research Program of China (Grant Nos. 2013CB933300), the International Science Technology Cooperation Program of China (Grant No. 2013DFR00730), and Jilin Provincial Natural Science Foundation (Grant Nos. 20140101203JC).

Author details

[1]State Key Laboratory of Luminescence and Applications, Changchun Institute of Optics, Fine Mechanics and Physics, Chinese Academy of Sciences, Changchun 130033, China. [2]School of Physics and Information Technology, Shaanxi Normal University, Xi'an 710062, China. [3]Centre for Advanced Optoelectronic Functional Materials Research and Key Laboratory for UV Light-Emitting Materials and Technology of Ministry of Education, Northeast Normal University, Changchun 130024, China.

Received: 17 December 2015 Accepted: 13 April 2016
Published online: 23 April 2016

References

1. Harris SE (1997) Topical review electromagnetically induced transparency. Phys Today 50:36–42
2. Marangos JP (1998) Electromagnetically induced transparency. J Mod Opt 45:471–503
3. Fleischhauer M, Imamoglu A, Marangos JP (2005) Electromagnetically induced transparency: optics in coherent media. Rev Mod Phys 77:633–673
4. Harris SE (1989) Lasers without inversion: interference of lifetime-broadened resonances. Phys Rev Lett 62:1033–1036
5. Mandel P (1993) Lasing without inversion—a useful concept. Contemp Physics 34:235–246
6. Mompart J, Corbalan R (2000) Lasing without inversion. J Opt B 2:R7–R24
7. Bergmann K, Theuer H, Shore BW (1998) Colloquium: coherently controlled adiabatic passage. Rev Mod Phys 70:1003–1025
8. Vitanov NV, Fleischhauer M, Shore BW, Bergmann K (2001) Perspective: stimulated Raman adiabatic passage: the status after 25 years. Adv At Mol Opt Phys 46:55–190
9. Kral P, Thanopulos I, Shapiro M (2007) Coherent population transfer among quantum states of atoms and molecules. Rev Mod Phys 79:53–77
10. Bergmann K, Vitanov NV, Shore BW (2015) Coherent manipulation of atoms and molecules by sequential laser pulses. J Chem Phys 142:170901
11. Hau LV, Harris SE, DuttonZ Behroozi CH (1999) Gain-assisted superluminal light propagation. Nature 397:594–598
12. Wang LJ, Kuzmich A, Dogariu A (2000) Light speed reduction to 17 metres per second in an ultracold atomic gas. Nature 406:277–279

13. Kuklinski JR, Gaubatz U, Hioe FT, Bergmann K (1989) Adiabatic population transfer in a three-level system driven by delayed laser pulses. Phys Rev A 40:6741–6744
14. Nakajima T, Lambropoulos P (1996) Population transfer through an autoionizing state by pulse delay. Z Phys D 36:17–22
15. Oreg J, Hioe FT, Eberly JH (1984) Coherent population transfer in multilevel systems with magnetic sublevels. II. Algebraic analysis. Phys Rev A 29:690–697
16. Coulston GW, Bergmann K (1992) Population transfer by stimulated Raman scattering with delayed pulses: analytical results for multilevel systems. J Chem Phys 96:3467–3475
17. Martin J, Shore BW, Bergmann K (1995) Adiabatic following in multilevel systems. Phys Rev A 52:583–593
18. Yang X, Zhu S (2008) Control of coherent population transfer via spontaneous decay-induced coherence. Phys Rev A 77:063822
19. Wang L, Song XL, Li AJ, Wang HH, Wei XG, Kang ZH, Jiang Y, Gao JY (2008) Coherence transfer between atomic ground states by the technique of stimulated Raman adiabatic passage. Opt Lett 33:2380–2382
20. Vitanov NV, Suominen KA, Shore BW (1999) Creation of coherent atomic superpositions by fractional stimulated Raman adiabatic passage. J Phys B-At Mol Opt 32:4535–4546
21. Niu Y, Gong S, Li R, Jin S (2004) Creation of atomic coherent superposition states via the technique of stimulated Raman adiabatic passage using a Λ-type system with a manifold of levels. Phys Rev A 70:023805
22. Kamada H, Gotoh H, Temmyo J, Takagahara T, Ando H (2001) Exciton Rabi oscillation in a single quantum dot. Phys Rev Lett 87:246401
23. Stievater TH, Li X, Steel DG, Gammon D, Katzer DS, Park D, Piermarocchi C, Sham JL (2001) Rabi oscillations of excitons in single quantum dots. Phys Rev Lett 87:133603
24. Htoon H, Takagahara Kulik TD, Baklenov O, Holmes ALA, Shih CK (2002) Interplay of Rabi oscillations and quantum interference in semiconductor quantum dots. Phys Rev Lett 88:087401
25. Zrenner A, Beham E, Stufler S, Findeis F, Bichler M, Abstreiter G (2002) Coherent properties of a two-level system based on a quantum-dot photodiode. Nature 418:612–614
26. Kim J, Benson O, Kan H, Yamamoto Y (1999) A single-photon turnstile device. Nature 397:500–503
27. Michler P, Kiraz A, Becher C, Schoenfeld WV, Petroff PM, Zhang L, Hu E, Imamoglu A (2000) A quantum dot single-photon turnstile device. Science 290:2282–2285
28. Cole BE, Williams JB, King BT, Sherwin MS, Stanley CR (2001) Coherent manipulation of semiconductor quantum bits with terahertz radiation. Nature 410:60–63
29. Wang L, Rastelli A, Kiravittaya S, Benyoucef M, Schmidt OG (2009) Self-assembled quantum dot molecules. Adv Mater 21:2601–2618
30. Bayer M, Hawrylak P, Hinzer K, Fafard S, Korkusinski M, Wasilewski ZR, Stern O, Forchel A (2001) Coupling and entangling of quantum states in quantum dot molecules. Science 291:451–453
31. Paspalakis E (2003) Localizing two interacting electrons in a driven quantum dot molecule. Phys Rev B 67:233306
32. Villas-Bôas JM, Ulloa SE, Govorov AO (2004) Coherent control of tunneling in a quantum dot molecule. Phys Rev B 69:125342
33. Krenner HJ, Sabathil M, Clark EC, Kress A, Schuh D, Bichler M, Abstreiter G, Finley JJ (2005) Direct observation of controlled coupling in an individual quantum dot molecule. Phys Rev Lett 4:057402
34. Unold T, Mueller K, Lienau C, Elsaesser T, Wieck AD (2005) Optical control of excitons in a pair of quantum dots coupled by the dipole-dipole interaction. Phys Rev Lett 94:137404
35. Stinaff EA, Scheibner M, Bracker AS, Ponomarev IV, Korenev VL, Ware ME, Doty MF, Reinecke TL, Gammon D (2006) Optical signatures of coupled quantum dots. Science 311:636–639
36. Boyer de la Giroday A, Sköld N, Stevenson RM, Farrer I, Ritchie DA, Shields AJ (2011) Exciton-spin memory with a semiconductor quantum dot molecule. Phys Rev Lett 106:216802
37. Kim D, Carter SG, Greilich A, Bracker AS, Gammon D (2011) Ultrafast optical control of entanglement between two quantum-dot spins. Nat Phys 7:223–229
38. Müller K, Bechtold A, Ruppert C, Zecherle M, Reithmaier G, Bichler M, Krenner HJ, Abstreiter G, Holleitner AW, Villas-Boas JM, Betz M, Finley JJ (2012) Electrical control of interdot electron tunneling in a double InGaAs quantum-dot nanostructure. Phys Rev Lett 108:197402
39. Weiss KM, Elzerman JM, Delley YL, Miguel-Sanchez J, Imamoğlu A (2012) Coherent two-electron spin qubits in an optically active pair of coupled InGaAs quantum dots. Phys Rev Lett 109:107401
40. Sköld N, Boyer de la Giroday A, Bennett AJ, Farrer I, Ritchie DA, Shields AJ (2013) Electrical control of the exciton fine structure of a quantum dot molecule. Phys Rev Lett 110:016804
41. Xie Q, Madhukar A, Chen P, Kobayashi NP (1995) Physics of lateral triple quantum-dot molecules with controlled electron numbers. Phys Rev Lett 75:2542–2545
42. Songmuang R, Kiravittaya S, Schmidt OG (2003) Vertically self-organized InAs quantum box islands on GaAs(100). Appl Phys Lett 82:2892–2894
43. Lee JH, Wang ZM, Strom NW, Mazur YI, Salamo GJ (2006) Formation of lateral quantum dot molecules around self-assembled nanoholes. Appl Phys Lett 89:202101
44. Chang-Yu H, Yun-Pil S, Marek K, Pawel H (2012) InGaAs quantum dot molecules around self-assembled GaAs nanomound templates. Rep Prog Phys 75:114501
45. Hayne M, Provoost R, Zundel MK, Manz YM, Eberl K, Moshchalkov VV (2000) Electron and hole confinement in stacked self-assembled InP quantum dots. Phys Rev B 62:10324–10328
46. Popescu V, Bester G, Hanna MC, Norman AG, Zunger A (2008) Theoretical and experimental examination of the intermediate-band concept for strain-balanced (In, Ga)As/Ga(As, P) quantum dot solar cells. Phys Rev B 78:205321
47. Tian SC, Wan RG, Tong CZ, Ning YQ, Qin L, Liu Y (2014) Giant Kerr nonlinearity induced by tunneling in triple quantum dot molecules. J Opt Soc Am B 31:1436–1442
48. Tian SC, Wan RG, Tong CZ, Ning YQ (2014) Controlling optical bistability via interacting double dark resonances in linear quantum dot molecules. J Opt Soc Am B 31:2681–2688
49. Sahrai M, Mehmannavaz MR, Sattari H (2014) Optically controllable switch for light propagation based on triple coupled quantum dots. Appl Opt 53:2375–2383
50. Hohenester U, Troiani F, Molinari E, Panzarini G, Macchiavello C (2000) Coherent electron transfer in a coupled quantum dot nanostructure using stimulated Raman adiabatic passage. Appl Phys Lett 77:1864–1866
51. Greentree AD, Cole JH, Hamilton AR, Hollenberg LCL (2004) Coherent electronic transfer in quantum dot systems using adiabatic passage. Phys Rev B 70:235317
52. Fountoulakis A, Paspalakis E (2013) Coherent population transfer in coupled semiconductor quantum dots. J Appl Phys 113:174301
53. Wu JH, Cui CL, Ba N, Ma QR, Gao JY (2007) Dynamical evolution and analytical solutions for multiple degenerate dark states in the tripod-type atomic system. Phys Rev A 75:043819